Journal of Neuroradiology 51 (2024) 101164

Available online at ScienceDirect www.sciencedirect.com

Elsevier Masson France EM|consulte www.em-consulte.com

Original Article

Multimodal assessment of brain fluid clearance is associated with amyloid-beta deposition in humans

Liangdong Zhou[†], Tracy A. Butler[†], Xiuyuan H. Wang, Ke Xi, Emily B. Tanzi, Lidia Glodzik, Gloria C. Chiang, Mony J. de Leon, Yi Li[*]

Department of Radiology, Brain Health Imaging Institute, Weill Cornell Medicine, 407 E 61st St, Feil 2, New York, NY 10065, United States

ARTICLE INFO

Article History:
Available online 30 October 2023

Keywords:
DTI-ALPS
CSF turnover rate vCSF
Brain clearance
Alzheimer's disease
^{11}C-PiB PET
Multimodal analysis
^{18}F-MK-6240 PET

ABSTRACT

Purpose: The present study investigates a multimodal imaging assessment of glymphatic function and its association with brain amyloid-beta deposition.
Methods: Two brain CSF clearance measures (vCSF and DTI-ALPS) were derived from dynamic PET and MR diffusion tensor imaging (DTI) for 50 subjects, 24/50 were Aβ positive (Aβ+). T1W, T2W, DTI, T2FLAIR, and ^{11}C-PiB and ^{18}F-MK-6240 PET were acquired. Multivariate linear regression models were assessed with both vCSF and DTI-ALPS as independent variables and brain Aβ as the dependent variable. Three types of models were evaluated, including the vCSF-only model, the ALPS-only model and the vCSF+ALPS combined model. Models were applied to the whole group, and Aβ subgroups. All analyses were controlled for age, gender, and intracranial volume.
Results: Sample demographics (N=50) include 20 males and 30 females with a mean age of 69.30 (sd=8.55). Our results show that the combination of vCSF and ALPS associates with Aβ deposition ($p < 0.05$, $R^2 = 0.575$) better than either vCSF ($p < 0.05$, $R^2 = 0.431$) or ALPS ($p < 0.05$, $R^2 = 0.372$) alone in the Aβ+ group. We observed similar results in whole-group analyses (combined model: $p < 0.05$, $R^2 = 0.287$; vCSF model: $p < 0.05$, $R^2 = 0.175$; ALPS model: $p < 0.05$, $R^2 = 0.196$) with less significance. Our data also showed that vCSF has higher correlation ($r = -0.548$) in subjects with mild Aβ deposition and DTI-ALPS has higher correlation ($r=-0.451$) with severe Aβ deposition subjects.
Conclusion: The regression model with both vCSF and DTI-ALPS is better associated with brain Aβ deposition. These two independent brain clearance measures may better explain the variation in Aβ deposition than either term individually. Our results suggest that vCSF and DTI-ALPS reflect complementary aspects of brain clearance functions.

Introduction

Brain clearance can be broadly defined as the removal of soluble waste generated from neuronal functioning and other processes via multiple, overlapping systems.[1–8] Glymphatic clearance refers to the system in which cerebrospinal fluid (CSF) mixes with interstitial fluid (ISF) in the perivascular space (PVS) surrounding blood vessels, thereby facilitating the removal of soluble proteins and metabolic wastes from the central nervous system. In glymphatic clearance CSF enters the brain along arterial PVS, exchanges with ISF, and then exits along venous PVS. This continuous movement of fluid helps to maintain brain health by preventing the accumulation of potentially harmful waste products, such as amyloid-beta (Aβ), a protein associated with Alzheimer's disease (AD).[9,10] Impaired brain CSF clearance causes soluble Aβ accumulation and aggregation into Aβ plaques in the extracellular space, and is a hallmark of AD.[11] Late-onset AD is characterized by an overall impairment in Aβ clearance, not Aβ production, [12] implying an underlying deficit in brain clearance could be key in the pathogenesis of AD.

Several neuroimaging methods have been tested to assess brain clearance in humans. Using MRI, the rate at which intrathecally injected gadolinium-based contrast travels from a lumbar site of injection to brain PVS can be monitored; this is considered one of the most direct measures of perivascular clearance obtainable in humans, yet is inappropriate for routine research use.[13–15] MRI can also track the movement of contrast injected intravenously into brain fluid

Abbreviations: CN, cognitively normal; MCI, mild cognitively impaired; DTI-ALPS, diffusion tensor imaging along perivascular space; vCSF, CSF turnover rate; LV, lateral ventricle; PVS, perivascular space; MRI, magnetic resonance imaging; fMRI, functional magnetic resonance imaging; PC-MRI, phase-contrast MRI; WM, cerebral white matter; WMH, white matter hyperintensity; ADmask, Amyloid beta deposition sensitive mask in brain of AD spectrum; ICV, intracranial volume; PVE, partial volume effect; Aβ, beta-amyloid protein; Tau, tau protein; SUVR, standard uptake value ratio

* Corresponding author.
E-mail address: yil4008@med.cornell.edu (Y. Li).
† These authors contributed equally to this work.

https://doi.org/10.1016/j.neurad.2023.10.009
0150-9861/

spaces, but this method is limited as gadolinium molecules are intentionally large to restrict entry to the brain or CSF/ISF spaces. One of the most promising MR methods is Diffusion Tensor Imaging along perivascular spaces (DTI-ALPS). DTI-ALPS quantifies the ratio of water diffusivity in the direction of PVS to the direction perpendicular to PVS and is expected to reflect the glymphatic function.[16,17] DTI-ALPS has demonstrated glymphatic dysfunction in AD [18,19] and other disorders.[20–22]

Dynamic Positron Emission Tomography (PET) is a promising tool for imaging the glymphatic system.[7,23–25] We developed a method to measure ventricular CSF clearance/turnover (vCSF) based on the rate of radiotracer removal from the lateral ventricle (LV).[7,26] This focus on radiotracer washout differs from the traditional use of PET that assesses radiotracer uptake or binding since there is no tracer binding in the LV. We used ^{18}F-MK-6240, a second-generation tau PET imaging agent, which has low molecular weight (505.5 g/mol) and freely crosses the blood–brain barrier.[27,28] It demonstrates higher signal-to-noise, no binding in choroid plexus, and in-vivo kinetics preferable to previous PET radioligands we have used in previous CSF clearance studies.[7,26] vCSF corresponds to the rate of decreasing radiotracer concentration in ventricular CSF normalized by the total amount of tracer delivery. It can also be measured using compartment modeling that provides convergent results.[24,25,29] vCSF is a net measure reflecting several processes critical to brain clearance of solutes: 1) directional flow of CSF (and tracer) within the ventricular system to the subarachnoid space for perivascular/glymphatic clearance, 2) CSF mixing/tracer dilution via pulsatile back-and-forth flow and diffusion within the ventricular system, and 3) tracer dilution via new CSF production (~18–25 ml/h [30]) and diffusion of ISF into the ventricle.[8,31,32] We have shown that vCSF is reduced in AD and correlates with Aβ deposition measured by ^{11}C-PiB PET.[7,26]

We hypothesize that DTI-ALPS and vCSF reflect different aspects of brain CSF clearance. Combining modalities should provide a more accurate and comprehensive understanding of a complex system involving interconnected brain fluid systems at multiple levels of the nervous system. Due to conflicting results of previous studies, showing that independent methods provide convergent information is important for cross validation of both methods as measures of brain clearance in humans. We therefore tested the ability of two noninvasive fluid clearance measures, vCSF and DTI-ALPS, independently and combined, to assess the extent of cortical Aβ deposition in a group of well-characterized subjects. Brain Aβ arguably constitutes the only established evidence of clearance failure in humans. Research gauging the accuracy and validity of clearance imaging methods is warranted.[33,34]

Materials and methods

Subjects

Sixty-nine subjects (age > 50 years) were recruited in this study. Subjects were recruited to this IRB approved study by advertising (community mailers or internet postings) and by physicians' referrals. Exclusions included: MRI evidence of stroke,[35] sleep disorder, probable Cerebral Amyloid Angiopathy (CAA),[36] and severe WM lesions (Fazekas=3);[37] subjects with STAGE 2 hypertension,[38] brain tumors, and other neoplastic disorders outside the brain where disease itself or its treatment (radiation, chemotherapy) is likely to affect brain structure or function. Exclusions are made for major depression indicated by scores ≥29 on the Beck Depression Inventory, developmental intellectual disability, and recent/ or active substance abuse. Subjects missing any required images (MR DTI, ^{11}C-PiB and ^{18}F-MK-6240 PET) were excluded (n=9). Also excluded were 4 subjects with hydrocephalus,[39] 1 with white matter lesion (Fazekas=3)[37], 1 with a sleep disorder, and 1 with microbleeding. 3 Aβ- subjects diagnosed as MCI were (PiB SUVR<1.23)[40] also excluded. A flow chart depicting exclusions is presented in Fig. 1.

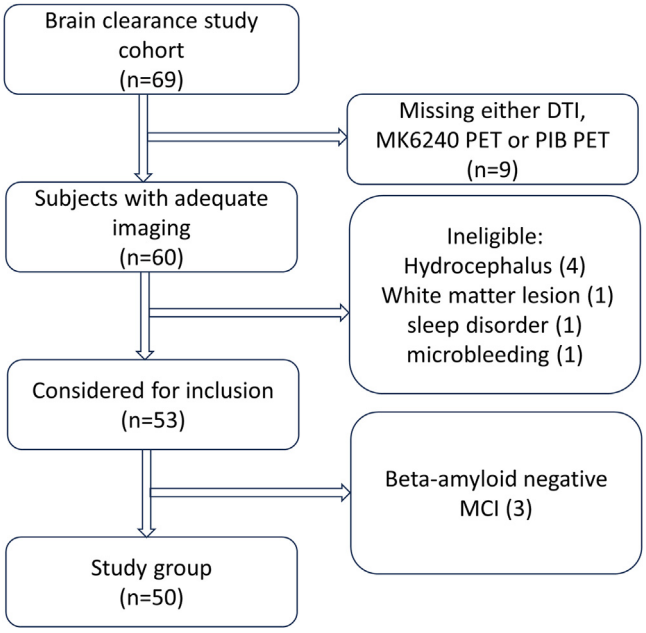

Fig. 1. Flowchart of participants finalization.

Subject assessment

Each subject underwent detailed evaluations by a cognitive neurologist consisting of a neurological exam, informant confirmed interviews, the Clinical Dementia Rating scale (CDR),[41] Montreal Cognitive Assessment (MoCA),[42] the National Alzheimer's Coordinating Committee's (NACC) telephone cognitive battery,[43] routine blood tests, ECG, MRI, and amyloid and tau PET. Subjects were assigned a final diagnosis according to NACC criteria based on all available information. Images were reviewed by a board certified neuroradiologist and assessed based on American College of Radiation criteria. Cases with uncertain diagnoses were presented at multidisciplinary consensus diagnostic meetings. The present study includes those diagnosed as cognitively normal (CN), mild cognitive impairment (MCI), or dementia due to AD.

MRI and PET acquisition

Subjects underwent MRI on a 3T Siemens Prisma scanner with a 64-channel head-neck coil. T1w used for co-registration and segmentation was acquired using MPRAGE sequence with TR/TE=2400/2.96ms, flip angle=9°, FOV=25.6 × 25.6cm, matrix size =256 × 256, 208 sagittal slices, voxel size=0.5 × 0.5 × 0.5mm. DTI used for computing DTI-ALPS (PVS clearance)[16] was acquired with 98 directions, TR/TE=3230/89.20ms, flip angle=78°, FOV=21 × 21cm, matrix size=140 × 140, voxel size=1.5 × 1.5 × 1.5mm, 92 axial slices, 3 b-values=0, 1500, and 3000s/mm2, multiband factor=6. Each DTI scan was acquired with opposite phase encoding direction for geometric distortion correction. T2w was acquired using T2-SPACE sequence with FOV=256 mm, TR/TE=3200/408ms, matrix size=512 × 512 with 320 sagittal slices, voxel size=0.5 × 0.5 × 0.5 mm3. FLAIR used for white matter hyperintensity (WMH) to determine a Fazekas scale rating was acquired with 1mm isotropic voxel size,[37] FOV=250 mm, TR/TE=7600/384ms. SWI used for checking micro-bleeding was acquired using multi-echo gradient echo sequence with 10 TEs from 6.1ms to 58.30ms, TR =63ms, FOV=256mm, matrix size=416 × 512 × 144, voxel size=0.5 × 0.5 × 1 mm3.

PET scanning used a Siemens Biograph mCT–S (64) slice PET/CT. ^{11}C-PiB was synthesized by the Weill Cornell Medicine radiochemistry facility. ^{18}F-MK6240 was provided by the manufacturer. ^{11}C-PiB PET data was acquired from 40-90 min after rapid bolus injection of ~555 MBq. ^{18}F–MK6240 data was acquired from 0-60 min and 90-120 min after rapid bolus injection of ~185 MBq with a break between acquisitions. ^{11}C-PiB PET images were reconstructed to a 512 × 512 × 74 matrix of 0.8 × 0.8 × 3 mm voxels in 5 × 10 min time frames from 40min to 90 min. ^{18}F-MK-6240 PET images were reconstructed to a 400 × 400 × 109 matrix of 1 × 1 × 2 mm voxels with 31 frames (12 × 10 seconds, 3 × 1 min, 10 × 5 min, 6 × 5 min).

Imaging processing

ROI parcellation

T1w MRI was segmented using FreeSurfer1 (FS)[44] version 7.1 recon-all command for ROI parcellation with assistance of T2w to enhance the segmentation quality. ROIs included the bilateral cerebellar cortex as a reference region to determine Aβ standard uptake value ratio (SUVR), and bilateral parietal, frontal and temporal ROIs, collectively referred to as the AD cortical mask (ADmask)[45] for quantifying Aβ. All ROIs were eroded one voxel from both sides using 3D sphere kernel to avoid partial volume effect (PVE). The intracranial volume (ICV) was measured using segmented brain mask (GM+WM +CSF) in SPM12.[46]

Evaluation of WMH

We evaluated white matter hyperintensity (WMH) severity and distribution in all subjects. We scored deep WMH (DWMH) and periventricular WMH (PVWMH) following Fazekas scale criteria.[37] Specifically, the WMH in periventricular white matter is categorized into 4 grades: 0=absent, 1=caps or pencil-thin lining, 2=smooth halo, and 3=irregular periventricular signal extending into the deep white matter; in deep white matter is scored as 0=absent, 1=punctate foci, 2=beginning confluence, and 3=large confluent areas.

PiB PET SUVR

Summed ^{11}C-PiB PET data from 60 min to 90 min were used for SUVR calculation. All the dynamic frames were realigned to the summed images between 40-90min, and the summed image was then coregistered to the T1w in FS space using boundary-based registration (bbr) method in FS.[47] SUVR was calculated by using the cerebellar cortex for reference. Average SUVR within the cortical ADmask served as the measure of Aβ deposition.[45] Subjects were classified as quantitatively Aβ+ or Aβ-using a cut-off value SUVR=1.23.[40]

^{18}F-MK-6240 vCSF

Dynamic ^{18}F-MK-6240 PET data from 0 min to 60 min was used for calculating brain CSF clearance in the lateral ventricle. All the dynamic frames were realigned to the summation of the frames between 6-30 min. The summation was then coregistered to the T1w in FS space using FSL with normalized mutual information (NMI) cost function and the coregistration transformation matrix was saved. The transformation matrix was then applied to all the dynamic frames to get dynamic ^{18}F-MK-6240 PET data in FS space. ^{18}F-MK-6240 PET SUVR was calculated using a summed image during 90 min to 120 min with a reference in the cerebellar cortex. Tau status (tau+/-) reading was performed on the MK SUVR by two experienced neuroradiologists (YL and GC).

The ventricular CSF clearance rate (vCSF) was measured by calculating the slope of the time-activity-curve (TAC) in an ROI consisting of 3-voxels eroded (2D disk kernel) in the lateral ventricle (LV) during 10min to 30min and normalized by the area under curve (AUC) of the whole brain TAC during 1 min to 4 min. Fig. 2 presents an illustrative description of the vCSF calculation and formula.

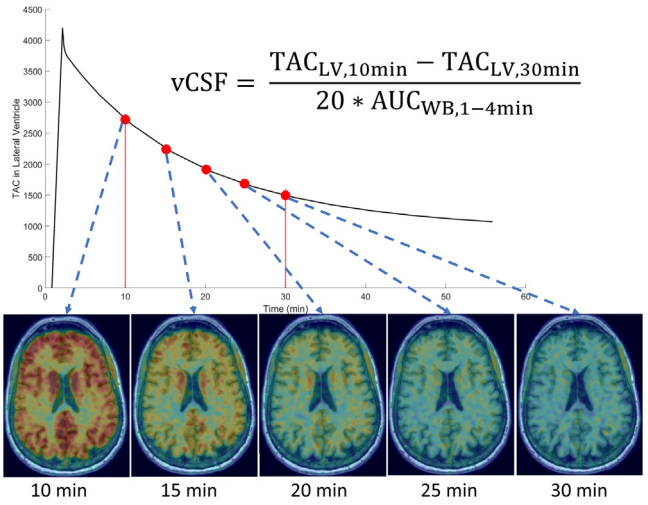

Fig. 2. Illustration of dynamic ^{18}F-MK6240 in the brain and formulation for calculation of vCSF using TAC in lateral ventricle and area under curve (AUC) of whole brain (WB) TAC.

DTI-ALPS

DTI data was corrected for susceptibility-induced geometric and eddy current distortions, and intervolume subject motion using the topup and eddy toolboxes in FSL.[48] The preprocessed dMRI data are used to fit diffusion tensors and obtain fractional anisotropy (FA) and diffusivity maps for each subject in the directions of the x- (right-left, D_{xx}), y- (anterior-posterior, D_{yy}), and z-axes (inferior-superior, D_{zz}). D_{xx} corresponds to the direction of vessels in the periventricular white matter, considered to reflect perivenous water diffusivity and glymphatic function.[16,17] On the color-coded FA map, 5-mm circle ROIs are placed bilaterally in the projection and association areas on axial slices at the level of the lateral ventricle body. As shown in Fig. 3 (A) the color-coded FA with marked ROIs, and (B) the susceptibility weighted image (SWI) showing medullary veins. Diffusivity values are calculated within each ROI. ALPS-index, reflecting CSF diffusivity in the direction of PVS, is calculated as: mean ($D_{xx,proj}$, $D_{xx,assoc}$)/mean ($D_{yy,proj}$, $D_{zz,assoc}$).[16,17] Left and right indices are averaged unless quantitative or visual differences e.g. due to lesion/injury are noted.

Statistical analysis

The relationship between Aβ deposition (PiB SUVR within the cortical AD ROI mask) and the clearance measurements (DTI-ALPS and vCSF) was evaluated using multiple regression models controlling for age, sex and ICV. The following regression models were tested (a) vCSF±ALPS model: PiBsuvr = b0 + b1*age + b2*sex + b3*vCSF + b4*ALPS + b5*vCSF*ALPS +b6*ICV; (b) vCSF only model: PiBsuvr = b0 + b1*age + b2*sex + b3*vCSF + b4*ICV and (c) ALPS only model: PiBsuvr = b0 + b1*age + b2*sex + b3*ALPS + b4*ICV. ICV term was included to control for head size, which may be related to brain clearance efficiency. An interaction term vCSF*ALPS in the vCSF+ALPS model was included to account for the interaction of two separate clearance functions from two distinct anatomical sites and medical imaging modalities. This approach will enable the evaluation of combining two clearance measures and could enhance the prediction of Aβ deposition than either measure alone.

The correlation between DTI-ALPS and vCSF was evaluated to check the concordance of two clearance measures using the Pearson or Spearman's rank correlation test depending on the data distribution. The age and sex effects of ALPS and vCSF were performed using a pairwise partial correlation by controlling for sex or age in both CN and MCI/AD groups.[49] To further test the effect of DTI-ALPS and vCSF on Aβ deposition in the Aβ+ group, we divided all Aβ+ subjects into

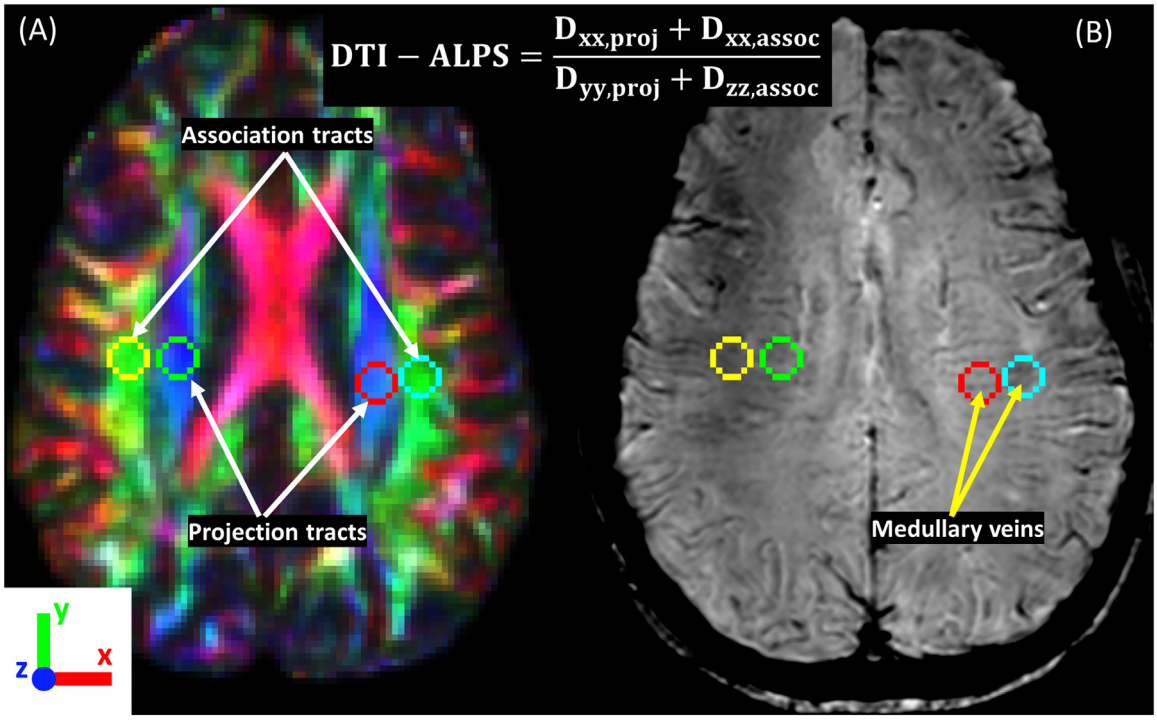

Fig. 3. Illustration of ROIs on (A) color-coded FA for DTI-ALPS, white matter fiber directions and (B) the medullary veins on SWI.

two groups of mild Aβ and severe Aβ deposition by using median PiB SUVR in cortical ADmask as cutoff. The correlation between PiB SUVR and DTI-ALPS and vCSF were performed by using Spearman's test in both mild and severe Aβ deposition groups. The effects of DWMH and PVWMH on vCSF, DTI-ALPS and Aβ deposition were tested by using a t-test or Kruskal-Wallis test for their group difference of all level of WMH scores, and Pearson or Spearman's tests were performed to check their correlation. The Shapiro-Wilk normality test was used to check the normality of the data before all the tests were performed.[50]

Whole-group and subgroup (Aβ+ and Aβ-) analyses were both conducted. The Akaike information criterion (AIC) and Bayesian information criterion (BIC) of the models were estimated for comparison. We further used the likelihood ratio test to compare the difference of nested models.[51]

Data availability

Data is available upon reasonable request with the provision of a formal data sharing agreement between the authors' and the requesting researchers' institutions.

Results

Demographics

Table 1 presents the demographic and diagnostic information of study subjects.

Table 1
Demographic and clinical information of subjects in this study.

Item	Number
Subjects number (n)	50
Gender: Male (%)	20 (40)
Mean Age (SD)	69.30 (8.55)
Diagnosis (%)	
Cognitive normal	34 (68)
MCI/AD	16 (32)
Aβ positive (%)	24 (48)
Tau positive (%)	17 (34)
DWMH score (%)	
0	14 (28)
1	29 (58)
2	6 (12)
3	1 (2)
PVWMH score (%)	
0	11 (22)
1	21 (42)
2	9 (18)
3	9 (18)

Effect of white matter hyperintensities

Spearman correlation tests show that PVWMH scores are correlated with DTI-ALPS ($r = -0.352$, $p < 0.05$) and vCSF ($r = -0.319$, $p < 0.05$) in the whole-group, but not PiB SUVR ($p > 0.05$). Kruskal-Wallis tests show group differences in DTI-ALPS differ by PVWMH scores ($\chi^2 = 9.158$, $p < 0.05$, mean of DTI-ALPS = 1.402, 1.432, 1.334, and 1.235 for PVWMH score 0, 1, 2, and 3, respectively). DWMH scores are neither correlated with DTI-ALPS nor vCSF ($p>0.05$).

All significant correlations and group differences lose significance after controlling for age and sex. Therefore, the WMH scores were not included in the following regression analysis.

Correlation between DTI-ALPS and vCSF

The Pearson's correlation between DTI-ALPS and vCSF is $r= 0.445$, $p < 0.01$ ($n=50$) in the whole group; $r = 0.560$, $p < 0.01$ ($n=24$) the β+ group; and $r = 0.311$, $p = 0.122$ ($n = 26$) and the Aβ- group. The results are presented in Fig. 4 as a scatter plot.

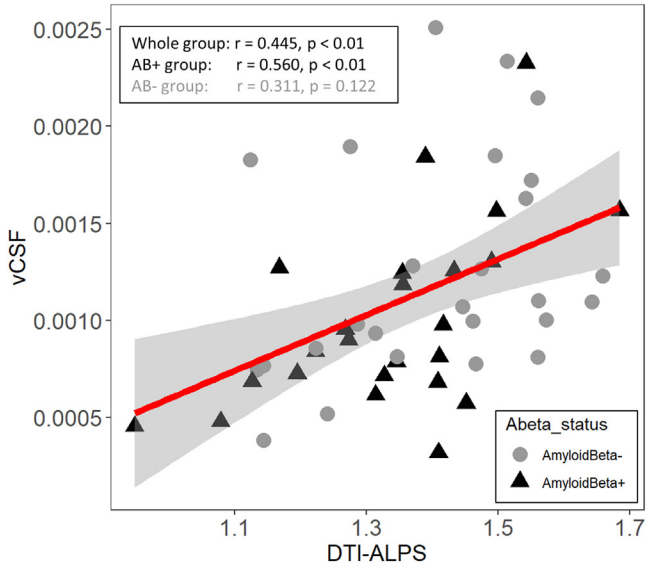

Fig. 4. The positive correlation between DTI-ALPS and vCSF. The correlation between them is the strongest in the Aβ+ group.

Age and sex effects of DTI-ALPS and vCSF

The age effects of vCSF, DTI-ALPS and PiB SUVR were assessed using the partial correlation by controlling for sex. Significant partial correlations between vCSF and age in CN ($r = -0.463$, $p < 0.05$), between ALPS and age in MCI ($r = -0.543$, $p < 0.05$), and between PiB SUVR and age in CN ($r = 0.358$, $p < 0.05$) were observed.

The sex effects of vCSF, DTI-ALPS and PiB SUVR were performed using the partial correlation by controlling for age. No correlations between these variables are significant in either CN or MCI/AD groups.

Association of Aβ deposition with both DTI-ALPS and vCSF based on Aβ status

In whole-group analyses of the vCSF-only model, only vCSF was significantly associated with PiB SUVR ($t = -2.221$, $p < 0.05$, $R^2 = 0.174$). In the ALPS-only model, only ALPS was significantly associated with PiB SUVR ($t = -2.488$, $p < 0.05$, $R^2 = 0.196$). In the vCSF +ALPS model ($R^2 = 0.286$), vCSF ($t = -2.468$, $p < 0.05$), ALPS ($t = -2.902$, $p<0.05$) and their interaction ($t = 2.334$, $p <0.05$) were all significantly associated with PiB SUVR. The partial regression plots for these significant variables in vCSF+ALPS model is presented in Fig. 5. The results show that both AIC (61.333 (vCSF+ALPS model) < 65.369 (ALPS model) < 66.609 (vCSF model)) and BIC (76.302 (vCSF+ALPS model) < 76.596 (ALPS model) < 77.837 (vCSF model)) for the combined model are smaller than the single clearance marker model. The likelihood ratio tests show that the vCSF+ALPS model is significantly better than vCSF-only ($\chi^2 = 7.872$, $p < 0.05$) and ALPS-only models ($\chi2 = 9.699$, $p < 0.05$).

For Aβ+ group analysis in the vCSF-only model, only vCSF was significantly associated with PiB SUVR ($t = -2.885$, $p < 0.05$, $R^2 = 0.431$, AIC = 32.571, BIC = 39.384.) In the ALPS-only model, only ALPS was significantly associated with PiB SUVR ($t = -2.416$, $p < 0.05$, $R^2 = 0.372$, AIC = 34.851, BIC = 41.664.) In the vCSF+ALPS model ($R^2 = 0.575$, AIC = 27.150, BIC = 36.234), vCSF ($t = -2.760$, $p < 0.05$), ALPS ($t = -2.843$, $p < 0.05$) and their interaction ($t = 2.533$, $p < 0.05$) as well as sex ($t = 2.450$, $p < 0.05$) were all significantly associated with PiB SUVR. The partial regression plots for these significant variables in the vCSF+ALPS model is presented in Fig. 6. The results show that both AIC (27.150 (vCSF+ALPS model) < 32.571 (vCSF model) < 34.851 (ALPS model)) and BIC (36.234 (vCSF+ALPS model) < 39.384 (vCSF model) < 41.644 (ALPS model)) for the combined model are smaller than the single clearance marker model. The likelihood ratio tests show that the vCSF+ALPS model is significantly better than the vCSF-only ($\chi^2 = 10.074$, $p < 0.05$) and the ALPS-only model ($\chi2 = 13.281$, $p < 0.05$).

For the Aβ- group, neither vCSF nor ALPS were significantly associated with PiB SUVR. Only age was significantly associated with the PiB SUVR in the ALPS-only model ($p<0.05$, Fig. 7 (C)), and marginally associated with PiB SUVR in vCSF-only ($p=0.056$, Fig. 7 (B)) and combined ($p=0.053$, Fig. 7 (A)) models. The likelihood ratio tests show no difference between the three models.

Association of Aβ deposition with both DTI-ALPS and vCSF based on Tau status

For the tau+ group, in the vCSF-only model ($n = 17$, $R^2 = 0.521$), both vCSF ($t = -2.58$, $p < 0.05$) and sex ($t = 2.199$, $p < 0.05$) are significantly associated with the PiB SUVR. In the ALPS-only model ($R^2 = 0.596$), both ALPS ($t = -3.184$, $p < 0.01$) and sex ($t = 2.645$, $p < 0.05$) are associated with PiB SUVR. In the vCSF+ALPS model ($R^2 = 0.599$), only sex ($t = 2.335$, $p < 0.05$) is significantly associated with PiB SUVR. ALPS is marginally associated with PiB SUVR ($t = -2.029$, $p = 0.070$). The likelihood ratio tests show that the vCSF+ALPS model is better than the vCSF model ($\chi2 = 6.146$, $p < 0.05$), but not significantly different from the ALPS model ($p > 0.05$).

For the tau- group, none of the investigated variables are significantly associated with PiB SUVR.

Correlation between clearance biomarkers (DTI-ALPS, vCSF) and Aβ deposition level

24 Aβ+ subjects were divided into two subgroups (12 mild and 12 severe Aβ deposition) by the median value of the global brain Aβ binding level (cut-off SUVR= 1.640). The correlation between PiB SUVR and DTI-ALPS is $r = -0.048$, and vCSF is $r = -0.548$ in mild Aβ group. For the severe Aβ group, the correlation between PiB SUVR and DTI-ALPS is -0.451, and vCSF is $r = -0.435$. These results show that vCSF is sensitive to mild Aβ deposition at early stage, while DTI-ALPS may capture severe Aβ accumulation.

Discussion

We found that two independent clearance measures, vCSF and DTI-ALPS, measured with ^{18}F-MK-6240 PET and MRI respectively, correlated strongly ($r = 0.560$ in Aβ+ group vs $r = 0.445$ in whole group), supporting both as in vivo measures of brain fluid clearance. We found that a model including both vCSF, DTI-ALPS, and their interaction term (controlling for age, sex and ICV) explained a remarkably high proportion of variance in cortical Aβ deposition (57.5%) in Aβ+ subjects. This model explained more variance (higher R^2 and lower AIC and BIC) than either clearance measure alone. Likelihood ratio tests show that the combination of vCSF and ALPS are significantly better associated with Aβ deposition in the Aβ+ and whole group than each individual model. vCSF and DTI-ALPS are clearance measures from different brain sites and quantified using different imaging modalities. The strong correlation between two independent clearance measures that collectively correlate with cortical amyloid – the only established gold standard of prior failed clearance - strongly supports their validity as in vivo clearance measures. Additionally, DTI-ALPS and vCSF independently explain variation in Aβ deposition, indicating that each measure reflects distinct, but complementary aspects of fluid clearance that can be applied to Aβ deposition and clearance. It is worth mentioning that this multimodal analysis with two clearance biomarkers will not impose any additional time or financial burden on patients since DTI MRI is a typical sequence in routine MRI scans, and vCSF derived from ^{18}F-MK-

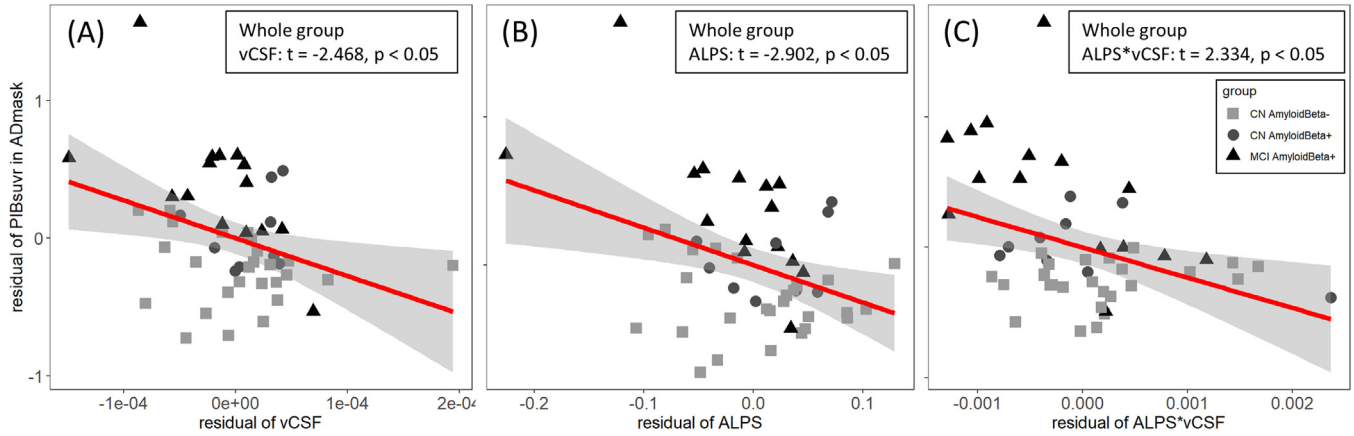

Fig. 5. In whole group, partial regression plot of significant variables versus Aβ deposit in AD mask in vCSF+ALPS model. (A) vCSF; (B) ALPS; and (C) ALPS*vCSF.

6240 PET is a second-generation tau PET imaging method typically required to confirm the diagnosis of AD.

The explanatory power increased dramatically for the Aβ+ group (57.5%) compared with the whole group consisting of Aβ+ and Aβ- subjects (only 28.6%). In Aβ- subjects, neither clearance measure explained cortical Aβ. These results are intuitive considering that subjects with significant, above-threshold Aβ accumulation demonstrate a clear, inverse relationship between clearance and Aβ is expected (i.e., worse clearance = higher Aβ). In contrast, in Aβ- subjects, the relationship between clearance and Aβ may be more complex, with clearance rates likely homeostatically linked to Aβ production/deposition in some, but not all subjects. Additionally,

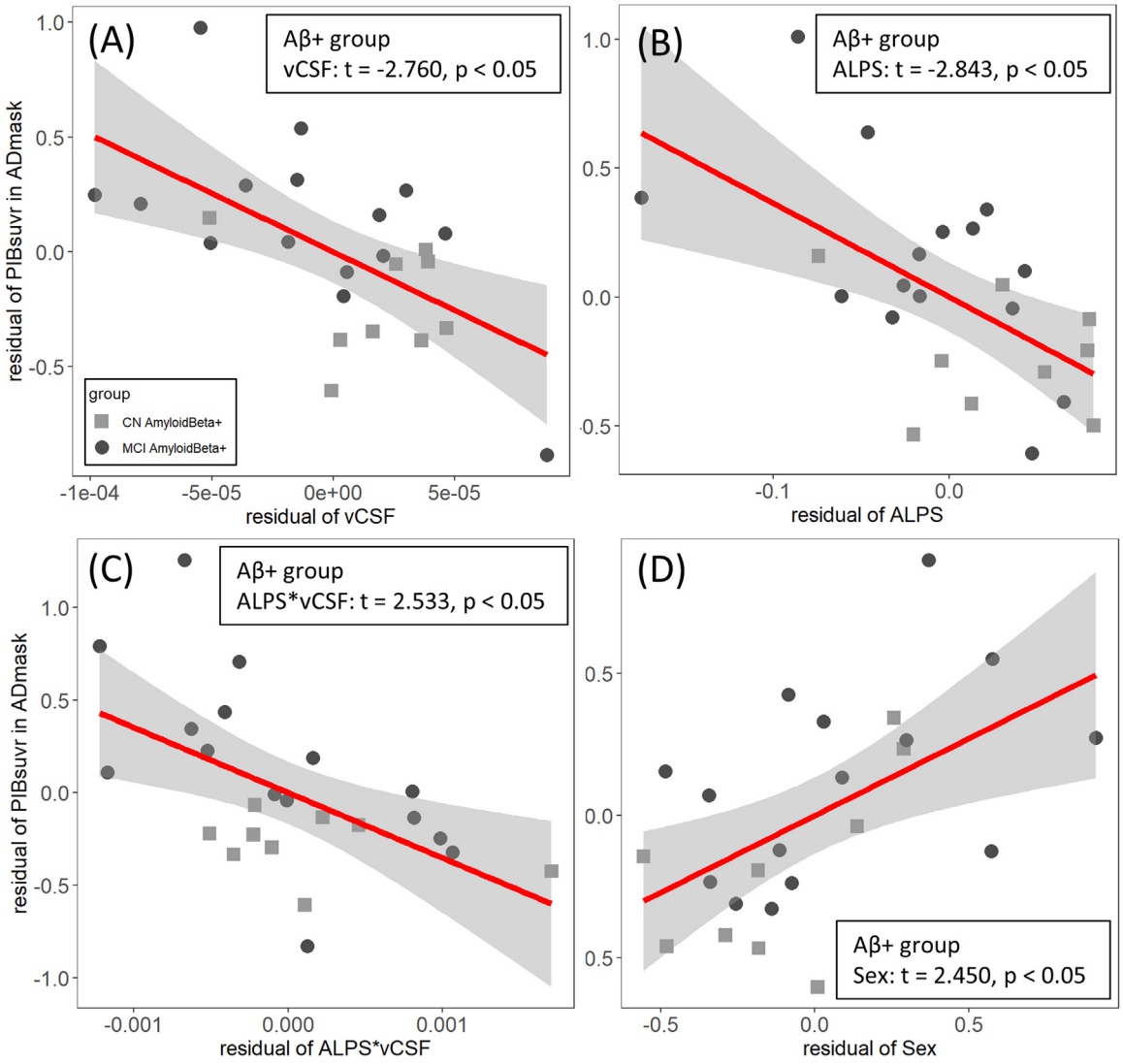

Fig. 6. In Aβ positive group, partial regression plot of significant variables versus Aβ deposit in AD mask in vCSF+ALPS model. (A) vCSF; (B) ALPS; (C) ALPS*vCSF; and (D) Sex.

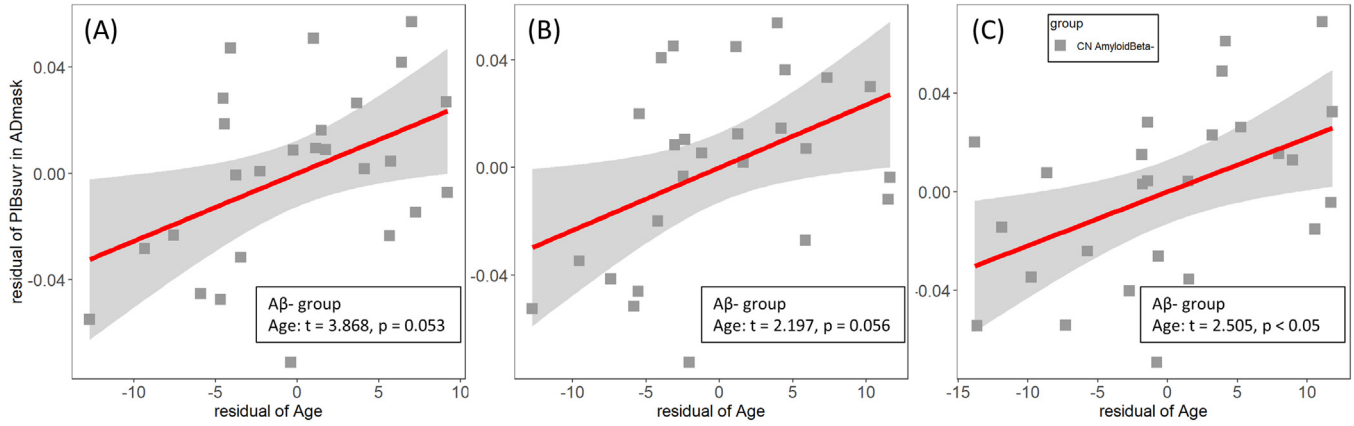

Fig. 7. In Aβ negative group, partial regression plot of significant variable (Age) versus Aβ deposit measured in AD mask in (A) vCSF+ALPS model, (B) vCSF model; and (C) ALPS model.

assessing the relationship between clearance and Aβ deposition in Aβ- subjects remains difficult because the total Aβ load is too low.

In all groups, when the models are divided by tau status instead of Aβ status results are weaker. However, we did observe a higher R-squared value for the vCSF-only and ALPS-only model compared with those from Aβ status-based model, implying a stronger correlation between the clearance measurements and Aβ deposition in tau+ group. Subjects with both Aβ and tau positivity are usually in a more advanced stage of the disease. One could infer that tau+ subjects may have stronger, measurable clearance deficits. CSF clearance deficits may also affect tau clearance and propagation in the brain.[52,53] Due to a limited number of tau+ subjects in our sample, further research is warranted to understand how brain clearance affects tau.

In the Aβ+ group, Pearson's correlation reveals that vCSF has a stronger correlation with Aβ deposition than ALPS in subjects with mild Aβ deposition, while ALPS has a stronger correlation in subjects with severe Aβ deposition. Mild Aβ deposition can be regarded as early Aβ deposition stage, while severe Aβ deposition may be treated as later Aβ deposition stage considering that Aβ accumulation is a gradual process. Note that in the Aβ+ group, R-squared for the vCSF-only model is 0.431, which is greater than the ALPS-only model (R^2=0.372), implying that vCSF and ALPS contain different and complementary information. This could explain why the combination model with both ALPS and vCSF is associated with Aβ deposition better than the individual markers. This could also be amongst the reasons why the combination model does not apply to the tau+ group in our data since most tau+ subjects (10/17) are in severe Aβ deposition group. Note that in the tau+ group, the R-squared for the vCSF-only model is 0.521 compared to 0.596 for ALPS-only model. Considering the results for the Aβ+ group and tau+ group together, the data shows that vCSF is a marker correlated with early clearance deficits while ALPS is more correlated with later clearance deficits. This could also imply that clearance deficits contribute to tau deposition, although further investigation is needed.

Glymphatic clearance depends on interconnected fluid systems. The recently characterized glymphatic system involves the convective exchange of CSF and ISF through PVS and the well-defined CSF system consisting of ventricles and connecting aqueducts. The interrelationship between bulk CSF flow and glymphatic flow has been widely discussed.[10,54,55] Abnormalities at any point within these interconnected systems may reduce CSF-ISF flow and mixing that in turn, impairs clearance of solutes like Aβ leading to its accumulation. Our data shows that both glymphatic function (DTI-ALPS) and ventricular CSF clearance/turnover (VCSF) are highly relevant to brain Aβ deposition. The ability to measure and monitor brain clearance in vivo in humans is expected to inform understanding of AD pathogenesis and guide targeted therapies.

Our data shows that WMH have no significant effects on Aβ deposition. However, PVWMH was observed negatively correlated with ALPS and vCSF. To reduce the effect of PVWMH on ALPS measures, we carefully avoided WMH regions when tracing ROIs for ALPS calculations in this study. ALPS and vCSF were calculated from different imaging modalities and by using unique algorithms. The negative correlation cannot be explained by WMH artifacts. It is unclear why PVWMH correlates to CSF clearance and DWMH does not, and this difference is likely induced by regional vulnerability. Periventricular white matter (PWM) is particularly susceptible to certain types of damage due to its blood supply and drainage dynamics. Being close to the ventricular system, any damage to the ependymal lining or changes in CSF dynamics might exert more direct effects on the PVWM and reactive astrogliosis might be more pronounced following such damage. Evaluating the relationship between WMH and ALPS or vCSF is out of the scope of this study. However, knowledge of this relationship will enhance the understanding of interacting neuroinflammation and brain CSF clearance.

Although the promising results presented in this study contribute to understanding brain clearance mechanisms in AD, it is not without limitations. First, this study includes a total of 50 subjects including 24 Aβ+ and 26 Aβ- subjects, with 16 Aβ+ subjects diagnosed as MCI/AD. Apply multimodal regression analyses and sub-analyses to a relatively small sample is difficult due to sample heterogeneity. An unbalanced sex ratio (30F+20M) along with an unbalanced sex distribution across ages (most Aβ+ male is between 65 to 80 years old) do not allow for rigorous analyses of sex differences in brain clearance. A larger sample is required to confirm these results. Second, as a cross-sectional study this research does not assess the causal effects that the two clearance markers may have on Aβ deposition longitudinally. These subjects are due for follow up assessments after two years. Third, the vCSF and ALPS are relatively new biomarkers in brain clearance research. In many studies, ALPS was considered a biomarker of interstitial fluid activity, and vCSF was developed as a marker of CSF turnover rate in the lateral ventricle. They are different from other proposed clearance measurements derived from functional MRI (fMRI) or phase-contract MRI (PC-MRI). PC-MRI quantifies rate, volume and direction of CSF transit through the ventricular system via the cerebral aqueduct.[56,57] fMRI has been used to assess physiological low-frequency oscillations that drive pulsatile CSF movement through the ventricular system into and out of the brain.[58,59] Future studies should test the convergent validity of our proposed framework with framework with fMRI, PC-MRI and other clearance measures.

Conclusion

Our results demonstrate that two independent brain clearance measures, MRI-quantified DTI-ALPS and PET-quantified vCSF,

correlate strongly. A regression model including both measures is associates with Aβ deposition more strongly than either measure alone. These results indicate that vCSF and ALPS reflect different and complementary aspects of the brain clearance system in humans. Reliable methods for measuring clearance in humans are essential in understanding how clearance dysfunction may lead to AD for early identification of reduced clearance in asymptomatic subjects at risk of neurodegeneration, and for testing the efficacy of interventions designed to enhance clearance and prevent disease.

Author contributions

LZ, TB, and YL: conceptualization. TB, and YL: study design. LZ, XH, and YL: imaging and data processing. LZ, KX and LG: analysis and statistics. LZ, TB, and YL: original draft. LZ, TB, XW, KX, ET, LG, GC, MJL and TL: review and editing. All authors contributed to the article and approved of the submitted version.

Funding

This work was supported by the National Institutes of Health (NIH) (R01 R56AG058913, R01 AG068398, AG057848, R01 AG022374, RF1 AG057570, R56 NS111052).

Declaration of Competing Interest

The authors have no competing interests to declare.

Acknowledgments

We thank the WCM radiochemistry team headed by Dr. James Kelly with the CBIC team (Drs. Stefan Guhlke, Keunpoong Lim, Nicole Waterhouse, Ruth Fernandez, Islami Besim, and Eva Burnazi) and Drs. Simon Morim, Jonathan P Dyke, and Edward K Fung for PET data collection, and Dr. Silky Pahlajani for clinical assessments. We also sincerely thank the anonymous reviewers for their insightful and thoughtful comments that greatly improved this manuscript.

References

1. Hladky SB, Barrand MA. Elimination of substances from the brain parenchyma: efflux via perivascular pathways and via the blood–brain barrier. *Fluids Barriers CNS*. 2018;15(1):30. https://doi.org/10.1186/s12987-018-0113-6.
2. Abbott NJ, Pizzo ME, Preston JE, Janigro D, Thorne RG. The role of brain barriers in fluid movement in the CNS: is there a “glymphatic” system? *Acta Neuropathol*. 2018;135(3):387–407. https://doi.org/10.1007/s00401-018-1812-4.
3. Bakker ENTP, Bacskai BJ, Arbel-Ornath M, et al. Lymphatic clearance of the brain: perivascular, paravascular and significance for neurodegenerative diseases. *Cell Mol Neurobiol*. 2016;36(2):181–194. https://doi.org/10.1007/s10571-015-0273-8.
4. Louveau A, Plog BA, Antila S, Alitalo K, Nedergaard M, Kipnis J. Understanding the functions and relationships of the glymphatic system and meningeal lymphatics. *J Clin Invest*. 2017;127(9):3210–3219. https://doi.org/10.1172/JCI90603.
5. Mestre H, Mori Y, Nedergaard M. The brain's glymphatic system: current controversies. *Trends Neurosci*. 2020;43(7):458–466. https://doi.org/10.1016/j.tins.2020.04.003.
6. Benveniste H, Liu X, Koundal S, Sanggaard S, Lee H, Wardlaw J. The glymphatic system and waste clearance with brain aging: a review. *GER*. 2019;65(2):106–119. https://doi.org/10.1159/000490349.
7. de Leon MJ, Li Y, Okamura N, et al. Cerebrospinal fluid clearance in alzheimer disease measured with dynamic PET. *J Nucl Med*. 2017;58(9):1471–1476. https://doi.org/10.2967/jnumed.116.187211.
8. Syková E, Nicholson C. Diffusion in brain extracellular space. *Physiol Rev*. 2008;88(4):1277–1340. https://doi.org/10.1152/physrev.00027.2007.
9. Iliff JJ, Wang M, Liao Y, et al. A paravascular pathway facilitates CSF flow through the brain parenchyma and the clearance of interstitial solutes, including amyloid β. *Sci Transl Med*. 2012;4(147). https://doi.org/10.1126/scitranslmed.3003748. 147ra111-147ra111.
10. Jessen NA, Munk ASF, Lundgaard I, Nedergaard M. The glymphatic system – a beginner's guide. *Neurochem Res*. 2015;40(12):2583–2599. https://doi.org/10.1007/s11064-015-1581-6.
11. Tarasoff-Conway JM, Carare RO, Osorio RS, et al. Clearance systems in the brain-implications for Alzheimer disease. *Nat Rev Neurol*. 2015;11(8):457–470. https://doi.org/10.1038/nrneurol.2015.119.
12. Mawuenyega KG, Sigurdson W, Ovod V, et al. Decreased clearance of CNS beta-amyloid in Alzheimer's disease. *Science*. 2010;330(6012):1774. https://doi.org/10.1126/science.1197623.
13. Eide PK, Valnes LM, Lindstrøm EK, Mardal KA, Ringstad G. Direction and magnitude of cerebrospinal fluid flow vary substantially across central nervous system diseases. *Fluids Barriers CNS*. 2021;18(1):16. https://doi.org/10.1186/s12987-021-00251-6.
14. Eide PK, Vinje V, Pripp AH, Mardal KA, Ringstad G. Sleep deprivation impairs molecular clearance from the human brain. *Brain*. 2021;144(3):863–874. https://doi.org/10.1093/brain/awaa443.
15. Ringstad G, Vatnehol SAS, Eide PK. Glymphatic MRI in idiopathic normal pressure hydrocephalus. *Brain*. 2017;140(10):2691–2705. https://doi.org/10.1093/brain/awx191.
16. Taoka T, Masutani Y, Kawai H, et al. Evaluation of glymphatic system activity with the diffusion MR technique: diffusion tensor image analysis along the perivascular space (DTI-ALPS) in Alzheimer's disease cases. *Jpn J Radiol*. 2017;35(4):172–178. https://doi.org/10.1007/s11604-017-0617-z.
17. Taoka T, Ito R, Nakamichi R, et al. Reproducibility of diffusion tensor image analysis along the perivascular space (DTI-ALPS) for evaluating interstitial fluid diffusivity and glymphatic function: changes in Alps index on multiple condition acquisition experiment (CHAMONIX) study. *Jpn J Radiol*. 2022;40(2):147–158. https://doi.org/10.1007/s11604-021-01187-5.
18. Hsu JL, Wei YC, Toh CH, et al. Magnetic resonance images implicate that glymphatic alterations mediate cognitive dysfunction in Alzheimer disease. *Ann Neurol*. 2023;93(1):164–174. https://doi.org/10.1002/ana.26516.
19. Kamagata K, Andica C, Takabayashi K, et al. Association of MRI indices of glymphatic system with amyloid deposition and cognition in mild cognitive impairment and Alzheimer disease. *Neurology*. 2022;99(24):e2648–e2660. https://doi.org/10.1212/WNL.0000000000201300.
20. McKnight CD, Trujillo P, Lopez AM, et al. Diffusion along perivascular spaces reveals evidence supportive of glymphatic function impairment in Parkinson disease. *Parkinsonism Relat Disord*. 2021;89:98–104. https://doi.org/10.1016/j.parkreldis.2021.06.004.
21. Si X, Guo T, Wang Z, et al. Neuroimaging evidence of glymphatic system dysfunction in possible REM sleep behavior disorder and Parkinson's disease. *npj Parkinsons Dis*. 2022;8(1):1–9. https://doi.org/10.1038/s41531-022-00316-9.
22. Carotenuto A, Cacciaguerra L, Pagani E, Preziosa P, Filippi M, Rocca MA. Glymphatic system impairment in multiple sclerosis: relation with brain damage and disability. *Brain*. 2022;145(8):2785–2795. https://doi.org/10.1093/brain/awab454.
23. Sigurdsson B, Hauglund NL, Lilius TO, et al. A SPECT-based method for dynamic imaging of the glymphatic system in rats. *J Cereb Blood Flow Metab*. February 21, 2023. https://doi.org/10.1177/0271678X231156982. Published online271678X231156982.
24. Schubert JJ, Veronese M, Marchitelli L, et al. Dynamic 11C-PIB PET shows cerebrospinal fluid flow alterations in Alzheimer disease and multiple sclerosis. *J Nucl Med*. 2019;60(10):1452–1460.
25. Turkheimer FE, Althubaity N, Schubert J, et al. Increased serum peripheral C-reactive protein is associated with reduced brain barriers permeability of TSPO radioligands in healthy volunteers and depressed patients: implications for inflammation and depression. *Brain Behav Immun*. 2021;91:487–497. https://doi.org/10.1016/j.bbi.2020.10.025.
26. Li Y, Rusinek H, Butler T, et al. Decreased CSF clearance and increased brain amyloid in Alzheimer's disease. *Fluids Barriers CNS*. 2022;19(1):21. https://doi.org/10.1186/s12987-022-00318-y.
27. Fu JF, Lois C, Sanchez J, et al. Further evaluation of 18F-MK-6240 reference region kinetics. *J Nucl Med*. 2021;62(supplement 1). 1058-1058.
28. Pascoal TA, Therriault J, Benedet AL, et al. 18F-MK-6240 PET for early and late detection of neurofibrillary tangles. *Brain*. 2020;143(9):2818–2830. https://doi.org/10.1093/brain/awaa180.
29. Althubaity N, Schubert J, Martins D, et al. Choroid plexus enlargement is associated with neuroinflammation and reduction of blood brain barrier permeability in depression. *Neuroimage Clin*. 2022;33: 102926. https://doi.org/10.1016/j.nicl.2021.102926.
30. Brown PD, Davies SL, Speake T, Millar ID. Molecular mechanisms of cerebrospinal fluid production. *Neuroscience*. 2004;129(4):957–970. https://doi.org/10.1016/j.neuroscience.2004.07.003.
31. Weller RO, Kida S, Zhang ET. Pathways of fluid drainage from the brain–morphological aspects and immunological significance in rat and man. *Brain Pathol*. 1992;2(4):277–284. https://doi.org/10.1111/j.1750-3639.1992.tb00704.x.
32. Bedussi B, van Lier MGJTB, Bartstra JW, et al. Clearance from the mouse brain by convection of interstitial fluid towards the ventricular system. *Fluids Barriers CNS*. 2015;12:23. https://doi.org/10.1186/s12987-015-0019-5.
33. Fagan AM, Mintun MA, Mach RH, et al. Inverse relation between in vivo amyloid imaging load and cerebrospinal fluid Abeta42 in humans. *Ann Neurol*. 2006;59(3):512–519. https://doi.org/10.1002/ana.20730.
34. McLean CA, Cherny RA, Fraser FW, et al. Soluble pool of Abeta amyloid as a determinant of severity of neurodegeneration in Alzheimer's disease. *Ann Neurol*. 1999;46(6):860–866. https://doi.org/10.1002/1531-8249(199912)46:6<860::aid-ana8>3.0.co;2-m.
35. Bamford J, Sandercock P, Dennis M, Warlow C, Burn J. Classification and natural history of clinically identifiable subtypes of cerebral infarction. *Lancet*.. 1991;337(Journal Article):1521–1526.
36. Greenberg SM, Charidimou A. Diagnosis of cerebral amyloid angiopathy. *Stroke*. 2018;49(2):491–497. https://doi.org/10.1161/STROKEAHA.117.016990.
37. Fazekas F, Chawluk JB, Alavi A, Hurtig HI, Zimmerman RA. MR signal abnormalities at 1.5 T in Alzheimer's dementia and normal aging. *AJR Am J Roentgenol*. 1987;149(2):351–356. https://doi.org/10.2214/ajr.149.2.351.

38. Chobanian AV, Bakris GL, Black HR, et al. Seventh report of the joint national committee on prevention, detection, evaluation, and treatment of high blood pressure. *Hypertension*. 2003;42(6):1206–1252. https://doi.org/10.1161/01.HYP.0000107251.49515.c2.
39. Evans Jr. WA. An encephalographic ratio for estimating ventricular enlargement and cerebral atrophy. *Arch Neurol Psychiatry*. 1942;47(6):931–937. https://doi.org/10.1001/archneurpsyc.1942.02290060069004.
40. Villeneuve S, Rabinovici GD, Cohn-Sheehy BI, et al. Existing Pittsburgh Compound-B positron emission tomography thresholds are too high: statistical and pathological evaluation. *Brain*. 2015;138(7):2020–2033. https://doi.org/10.1093/brain/awv112.
41. Morris JC. The Clinical Dementia Rating (CDR): current version and scoring rules. *Neurology*. 1993;43(11). https://doi.org/10.1212/WNL.43.11.2412-a. 2412-a.
42. Nasreddine ZS, Phillips NA, Bédirian V, et al. The montreal cognitive assessment, MoCA: a brief screening tool for mild cognitive impairment. *J Am Geriatr Soc*. 2005;53(4):695–699. https://doi.org/10.1111/j.1532-5415.2005.53221.x.
43. Besser L, Kukull W, Knopman DS, et al. Version 3 of the National Alzheimer's coordinating center's uniform data set. *Alzheimer Dis Assoc Disord*. 2018;32(4):351–358. https://doi.org/10.1097/WAD.0000000000000279.
44. Fischl B. FreeSurfer. *Neuroimage*. 2012;62(2):774–781. https://doi.org/10.1016/j.neuroimage.2012.01.021.
45. Mosconi L, Rinne JO, Tsui WH, et al. Increased fibrillar amyloid-β burden in normal individuals with a family history of late-onset Alzheimer's. *Proc Natl Acad Sci U S A*. 2010;107(13):5949–5954. https://doi.org/10.1073/pnas.0914141107.
46. Ashburner J, Friston KJ. Unified segmentation. *Neuroimage*. 2005;26(3):839–851. https://doi.org/10.1016/j.neuroimage.2005.02.018.
47. Greve DN, Fischl B. Accurate and robust brain image alignment using boundary-based registration. *Neuroimage*. 2009;48(1):63–72. https://doi.org/10.1016/j.neuroimage.2009.06.060.
48. Andersson JLR, Sotiropoulos SN. An integrated approach to correction for off-resonance effects and subject movement in diffusion MR imaging. *Neuroimage*. 2016;125:1063–1078. https://doi.org/10.1016/j.neuroimage.2015.10.019.
49. Kim S. ppcor: An R package for a fast calculation to semi-partial correlation coefficients. *Commun Stat Appl Methods*. 2015;22(6):665–674. https://doi.org/10.5351/CSAM.2015.22.6.665.
50. Shapiro SS, Wilk MB. An analysis of variance test for normality (complete samples). *Biometrika*. 1965;52(3/4):591–611. https://doi.org/10.2307/2333709.
51. Lv J, Fan Y. A unified approach to model selection and sparse recovery using regularized least squares. *Ann Stat*. 2009;37(6A):3498–3528.
52. Harrison IF, Ismail O, Machhada A, et al. Impaired glymphatic function and clearance of tau in an Alzheimer's disease model. *Brain*. 2020;143(8):2576–2593. https://doi.org/10.1093/brain/awaa179.
53. Ishida K, Yamada K, Nishiyama R, et al. Glymphatic system clears extracellular tau and protects from tau aggregation and neurodegeneration. *J Exp Med*. 2022;219(3): e20211275. https://doi.org/10.1084/jem.20211275.
54. Akins PT, Guppy KH. Does impaired glymphatic drainage cause glymphedema? A review tailored to neurocritical care and neurosurgery. *Neurocrit Care*.. June 10, 2021. https://doi.org/10.1007/s12028-021-01224-1. Published online.
55. Schubert JJ, Veronese M, Marchitelli L, et al. Dynamic 11C-PiB PET shows cerebrospinal fluid flow alterations in Alzheimer disease and multiple sclerosis. *J Nucl Med*. 2019;60(10):1452–1460. https://doi.org/10.2967/jnumed.118.223834.
56. Sakhare AR, Barisano G, Pa J. Assessing test-retest reliability of phase contrast MRI for measuring cerebrospinal fluid and cerebral blood flow dynamics. *Magn Reson Med*. 2019;82(2):658–670. https://doi.org/10.1002/mrm.27752.
57. El Sankari S, Gondry-Jouet C, Fichten A, et al. Cerebrospinal fluid and blood flow in mild cognitive impairment and Alzheimer's disease: a differential diagnosis from idiopathic normal pressure hydrocephalus. *Fluids Barriers CNS*. 2011;8(1):12. https://doi.org/10.1186/2045-8118-8-12.
58. Fultz NE, Bonmassar G, Setsompop K, et al. Coupled electrophysiological, hemodynamic, and cerebrospinal fluid oscillations in human sleep. *Science*. 2019;366(6465):628–631. https://doi.org/10.1126/science.aax5440.
59. Gonzalez-Castillo J, Fernandez IS, Handwerker DA, Bandettini PA. Ultra-slow fMRI fluctuations in the fourth ventricle as a marker of drowsiness. *Neuroimage*. 2022;259: 119424. https://doi.org/10.1016/j.neuroimage.2022.119424.